ELSEVIER

Ceramics International 27 (2001) 291–298

CERAMICS INTERNATIONAL

www.elsevier.com/locate/ceramint

Raman spectral characterization of existing phases in the ZrO_2–Y_2O_3–Nb_2O_5 system

Deuk Yong Lee [a,*], Joo-Wung Jang [b], Dae-Joon Kim [c]

[a] *Department of Metallurgical and Materials Engineering, Daelim College of Technology, Anyang 431-715, South Korea*
[b] *Dental Material Research Center, We Dong Myung Co., Ltd., KwangMyung 423-060, South Korea*
[c] *Materials Research Division, Korea Institute of Science and Technology, Seoul 136-791, South Korea*

Received 23 February 2000; received in revised form 21 March 2000; accepted 27 April 2000

Abstract

Tetragonal zirconia polycrystals (TZPs) were prepared with additions of 5.31 mol% Y_2O_3 plus up to 5 mol% Nb_2O_5 and their existing phases were investigated by Raman spectroscopy and X-ray diffraction. The present study reveals that Raman spectroscopy can identify the existing phases of cubic (c)-, tetragonal (t)-, monoclinic (m)-ZrO_2, and Y–Nb ordered phase. The phase stability of t-ZrO_2 may be governed by the competition between stable and transformable t-phase as a function of Nb_2O_5 content. Raman spectra of TZPs exhibit a broad and diffuse peak at around 770 cm^{-1} in contrast to the c-, t- and m-phases due to local ordering. The local environment of Nb^{5+} in this system is maintained throughout Nb_2O_5 concentrations ($0 < Nb_2O_5 \leqslant 5$ mol%), indicating that the 770 cm^{-1} mode is likely to be related to the stable t-phase.

Keywords: Tetragonal zirconia polycrystal; Y–Nb ordering; Raman spectroscopy

1. Introduction

Tetragonal zirconia polycrystals (TZPs) have been focused on as the candidate material of choice for structural and bio-ceramic applications, because of their excellent mechanical properties, hydrothermal phase stability, and biocompatibility [1–3]. Our previous work indicated that the stable TZPs exist in the composition region with 14–15 mol% $YNbO_4$ in the ZrO_2–$YNbO_4$ quasibinary system and within the certain triangular compositional boundary in the ZrO_2–Y_2O_3–Nb_2O_5 system [1].

In the ZrO_2–Y_2O_3–Nb_2O_5 system, as the Nb_2O_5 content increased up to 1.5 mol%, the rate of low-temperature degradation (LTD) rose due to the increase in the c/a axial ratio (tetragonality) of the t-ZrO_2 solid solution, associated with the internal strain, as a result of annihilation of oxygen vacancies introduced by Y^{3+} [4–6]. On the other hand, TZPs, having a composition of 90.24 mol% ZrO_2; 5.31 mol% Y_2O_3; 4.45 mol% Nb_2O_5 (5.31Y–TZP), showed excellent phase stability and fracture toughness due to local Y–Nb dopant ordering in t-ZrO_2 into a scheelite-like arrangement, which resulted in a relief of the internal strain in the t-ZrO_2 lattice [1,5–8]. In the ordered structure, the smaller cation Nb^{5+} adopts a four-fold coordination leaving eight-fold coordination to Y^{3+}, determined by the observation of X-ray absorption spectroscopy [7].

However, although it appears that another factor must be related to the aging behavior in these TZPs, no systematic study for the effect of Nb_2O_5 alloying to 5.31 mol% Y_2O_3–TZP on aging-induced degradation has been attempted over the composition range of Nb_2O_5, 0–5 mol%. For such purposes, detailed studies such as dependence of Nb_2O_5 alloying on existing phases were carried out by using Raman spectroscopy.

2. Experimental procedure

The powder preparation procedure of Y–TZP doped with Nb_2O_5 was reported elsewhere [1]. The powders

* Corresponding author. Tel.: +82-31-4674835; fax: +82-31-4674830.
E-mail address: dylee@daelim.ac.kr (D.Y. Lee).

0272-8842/01/$20.00
PII: S0272-8842(00)00079-1

having a composition of (94.69−x) mol% ZrO_2; 5.31 mol% Y_2O_3; x mol% Nb_2O_5 ($x=0$, 1, 2, 3, 4, and 5) were chosen for this study because TZP, having a composition of 90.24 mol% ZrO_2; 5.31 mol% Y_2O_3; 4.45 mol% Nb_2O_5, showed excellent phase stability.

The powders were isostatically pressed at 140 MPa into pellets and then sintered for 1 h at 1550°C with a heating rate of 6°C/min from room temperature to 900°C and 3°C/min up to the sintering temperature and then furnace cooled to room temperature. A typical dimension of the sintered specimens were 18 mm in diameter and 2.0 mm in thickness. The sintered density was measured by the Archimedes method, using distilled water as the immersion medium. The average grain size was measured from scanning electron micrographs by the linear intercept method with the use of a correction factor of 1.56 after Mendelson [9].

The strength of 5.31 mol% Y_2O_3 stabilized TZP (5.31Y–TZP) ceramics doped with Nb_2O_5 was evaluated by biaxial flexure testing [10]. Biaxial flexure disks were initially ground on both sides to a nominal thickness of 1.8 mm, polished to a 1 μm diamond finish and then subsequently annealed for 1 h at 1200°C in air. The disks were placed on a test fixture consisting of a three-point support and a loading plunger having a flat central loading point, and broken at a stress rate of 23 MPa s^{-1} (Instron 4465). The fracture toughness was determined by the indentation-strength method proposed by Chantikukl et al. [11]. A Vickers indent of 490 N was placed on the center of the tensile face of five test specimens. A drop of silicon oil was applied to minimize the moisture assisted subcritical crack growth. The ratio of hardness to modulus (H/E) was then determined by measuring Knoop indentation impression dimensions as reported by Marshall et al. [12]. The average strength data obtained from five specimens which fractured from the indented sites were used for the subsequent toughness determination.

The samples were aged for 500 h at 220°C in air and then the extent of LTD was estimated from the m-ZrO_2 fraction of the aged and the fractured specimens according to Garvie and Nicholson [13] using a X-ray diffractometer. For the determination of lattice parameter at room temperature, X-ray diffraction (XRD) data were obtained from the ground powders, mixed carefully with the silicon internal standard (SRM 640b, National Institute of Standards and Technology, Gaitherburg, MD), using an automated XRD (Philips, EA, Almelo, The Netherlands) with Cukα radiation (λ (Cukα_1)) = 0.154060 nm (1.54060 Å). A scan speed of 0.5° $2\theta/min^{-1}$ was used in the 2θ range of 65 to 120°.

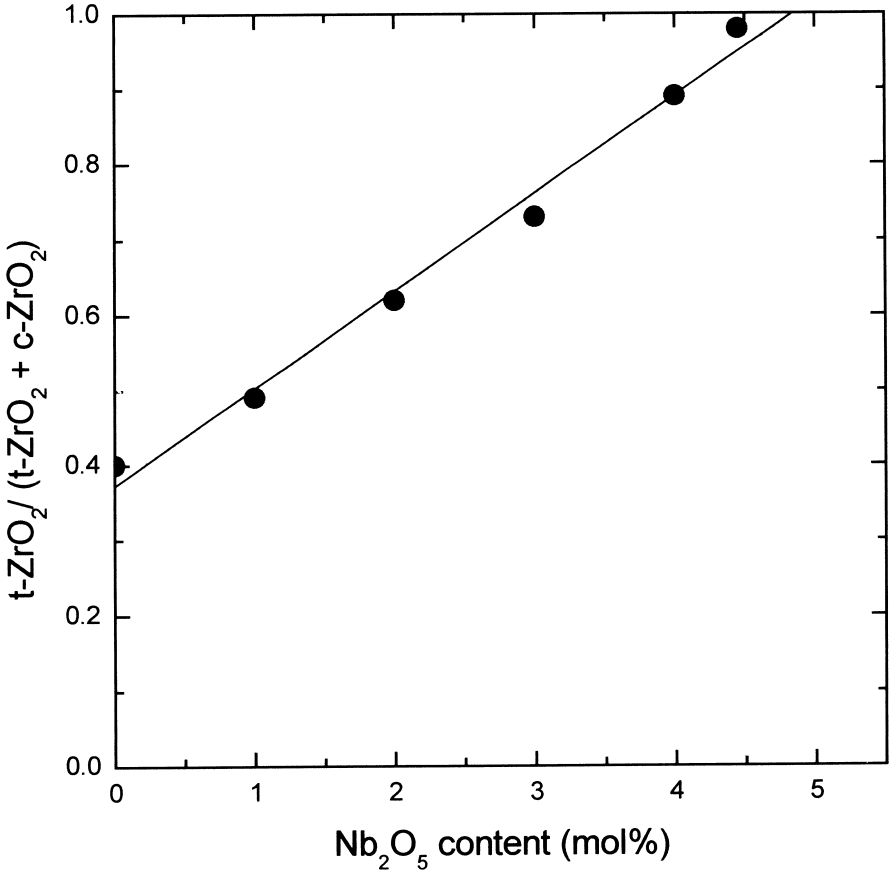

Fig. 1. Fraction of t-ZrO_2 of the sintered specimens having a composition of (94.69−x) mol% ZrO_2; 5.31 mol% Y_2O_3; x mol% Nb_2O_5 ($x=1$–4.45). The specimens were sintered for 1 h at 1550°C in air.

After $k\alpha_2$ peak stripping, the peak position was determined by profile refinement using the built-in PC-APD program. Details of the lattice parameter refinement procedure have been described elsewhere [14].

Raman Spectra were obtained by a double monochromator (Model U1000, Jobin Yvon, Longjumeau, France) in a backscattering geometry. The spectra were excited with an argon ion laser that was operating at a wavelength (λ) of 514.5 nm. Spectra of each specimen were taken over the range of 100–900 cm^{-1}, scanning at a step size of 1.0 cm^{-1} with an integration time constant of 1 s. The instrument was calibrated with the 520.9 cm^{-1} Raman band of silicon wafer, and the error in determining the peak shifts was ± 1 cm^{-1}. The wavenumbers of the Raman bands were determined by the Lorentzian curve fitting of the spectra.

3. Results and discussion

The sintered specimens having a composition of (94.69−x) mol% ZrO_2; 5.31 mol% Y_2O_3; x mol% Nb_2O_5 ($x=0$–5) are inhomogeneous due to the phase separation into t+c phases, as shown in Fig. 1. However, 5.31Y–TZP containing more than 4.6 mol% Nb_2O_5 could not be fabricated because of the nearly complete transformation to the m-ZrO_2 phase during cooling below 500°C. 5.31Y–TZP is composed of 40% t-phase and 60% c-phase, but the extent of t-phase rises linearly with increasing the Nb_2O_5 concentration, indicating that the c-phase becomes unstable and then decomposes into a t-phase. 5.31Y–TZPs doped with 4.45 to 4.6 mol% Nb_2O_5 show only t-phase. Unlike Y^{3+} and Zr^{4+}, Nb^{5+} is likely to occupy the four-fold coordination with oxygen ions due to the smaller ionic size of 0.074 nm [7], representing that the addition of Nb_2O_5 into 5.31Y–TZP destabilizes the c-phase due to the increased tetragonality (c/a ratio) as shown in Fig. 1.

The lattice parameters of 5.31Y–TZP are plotted as a function of the Nb_2O_5 concentration as shown in Fig. 2. In this system, it is believed that the lattice parameters should be constant regardless of the Nb_2O_5 content because these compositions are positioned inside the two-phase region [1]. However, the lattice paramters

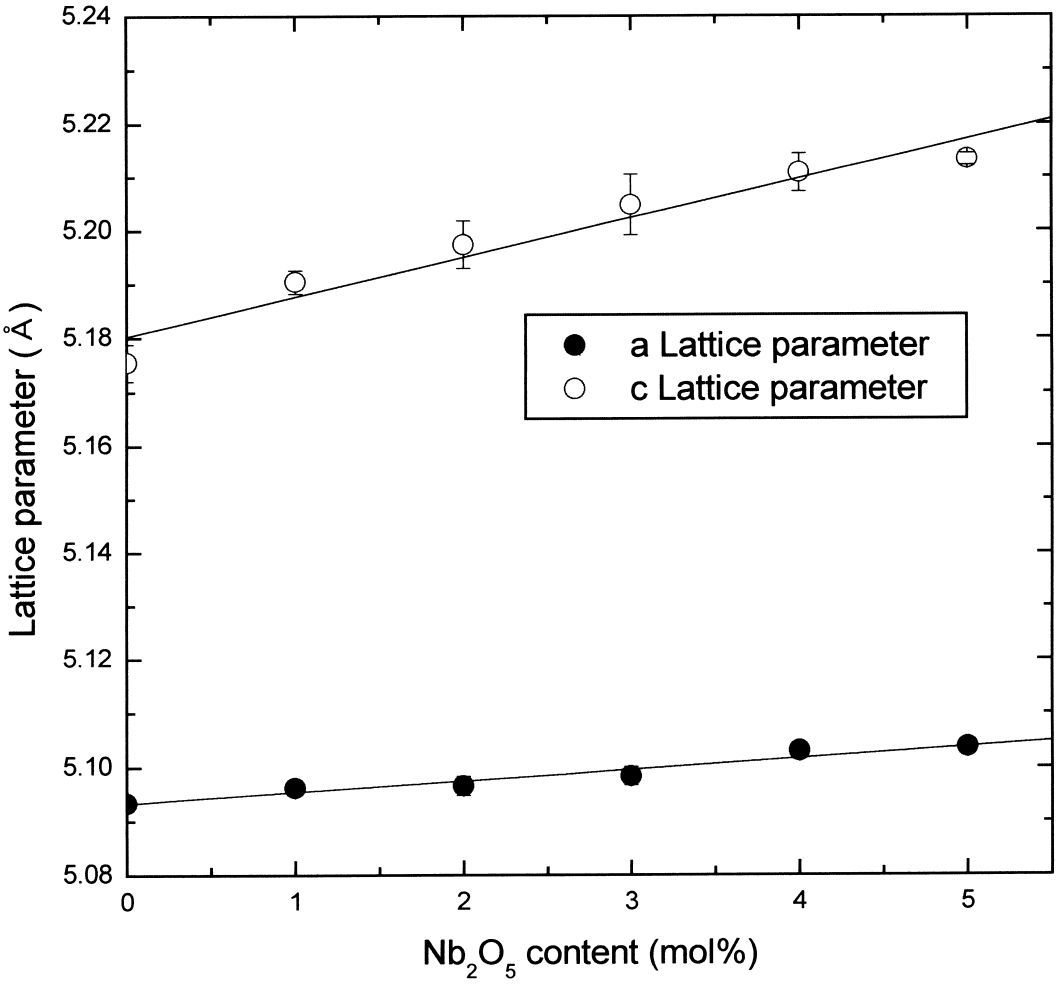

Fig. 2. Lattice parameters of 5.31 mol% Y_2O_3-stabilized ZrO_2 as a function of Nb_2O_5 content.

increase linearly with an increase in Nb_2O_5 content. Both lattice constants increase with the Nb_2O_5 addition, but the effect of Nb_2O_5 alloying on the c-axis lattice constants is more pronounced compared with the changes in the a-lattice parameter. This irrelevancy suggests that the stable t-ZrO_2 having a different crystal structure from the t-ZrO_2 existing in the ZrO_2–Y_2O_3 system may start to form from the c-phase with an increase in Nb_2O_5 content, however, the dissimilarity between two types of t-ZrO_2 solid solutions can not be discriminated by the XRD patterns.

The m-ZrO_2 content of the aged 5.31Y–TZP doped with Nb_2O_5 was measured by using XRD. At low concentrations, 0–3 mol%, both destabilized t-ZrO_2 and c-ZrO_2 may transform to transformable (degradable) t-ZrO_2 with increasing the Nb_2O_5 concentration, due to the annihilation of oxygen vacancies as a result of the substitution of Nb^{5+} for Zr^{4+}, as shown in Fig. 3. The degradable t-ZrO_2 in 5.31Y–TZP doped with 0–3 mol% Nb_2O_5 can be easily distorted so that such a distortion raises the internal strain, which is prerequisite for the t→m phase transformation. From 3 mol% Nb_2O_5, the fraction of m-ZrO_2 starts to decrease abruptly and then only t-ZrO_2 exists over the composition range of 4.45–4.6 mol% Nb_2O_5. The absence of LTD in 5.31Y–TZP doped with 4.45–4.6 mol% Nb_2O_5 indicates that two types of t-ZrO_2 phases, a stable t-ZrO_2 in the system ZrO_2–$YNbO_4$ and a degradable t-ZrO_2 in the system ZrO_2–Y_2O_3, may coexist, but the stable t-ZrO_2 phase hampers the t→m phase transformation of the degradable t-phase. That is, lattice relaxation of the degradable t-ZrO_2 is restrained significantly by the stable t-phase. It was reported by one of the authors that the stable t-ZrO_2, which does not transform to m-ZrO_2 during low-temperature aging, exists due to local Y–Nb ordering in the composition region with 14–15 mol% $YNbO_4$ in the ZrO_2–$YNbO_4$ quasibinary system [1]. At 4.45 mol% Nb_2O_5, Nb^{5+} necessary for the stability of t-ZrO_2 is dissipated by the proper substitution so that Y–Nb dopant ordering into a scheelite-like structure is achieved and the relaxation of the internal strain inherent in the t-lattice is accomplished. Beyond 4.6 mol% Nb_2O_5, the fraction of m-ZrO_2 starts to increase again, implying that the addition of excess Nb^{5+} into t-ZrO_2 increases the internal strain more significantly than TZPs doped with a small amount of Nb_2O_5 (0–3 mol%).

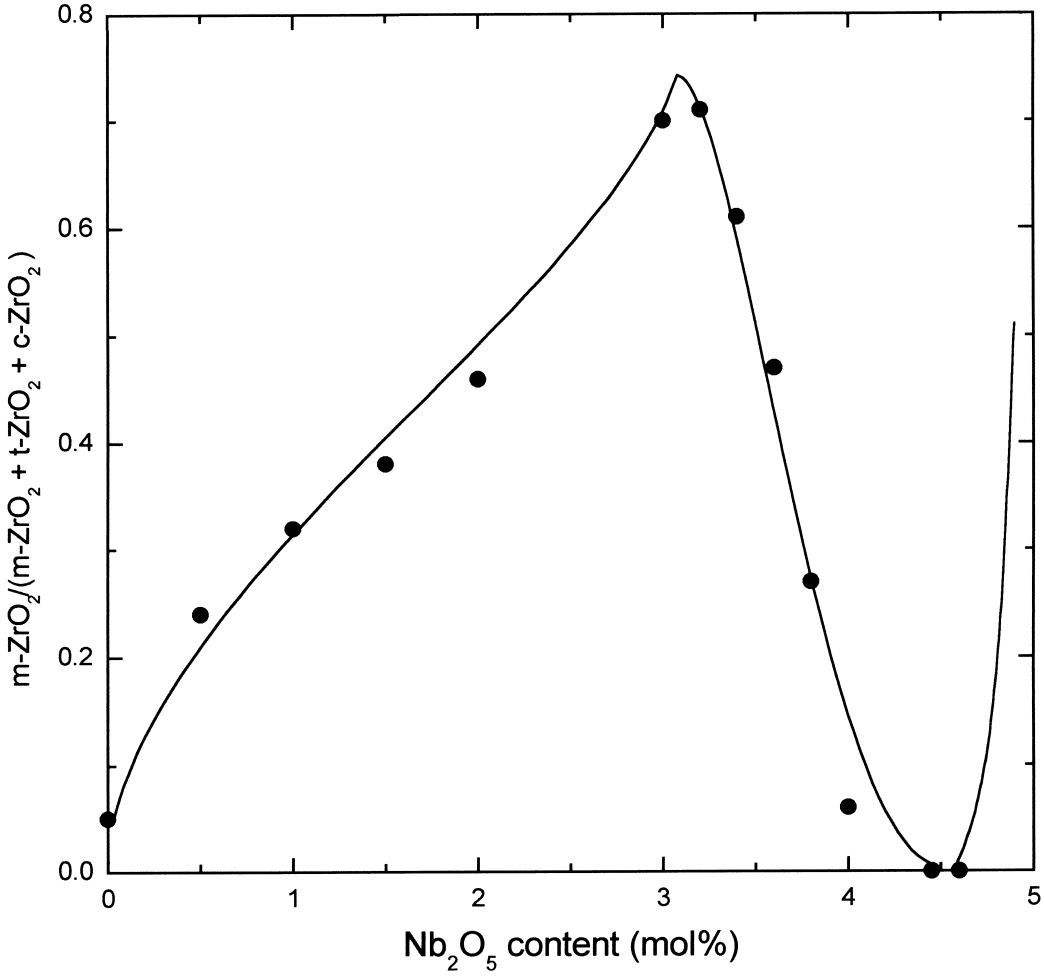

Fig. 3. m-ZrO_2 content of 5.31 mol% Y_2O_3-stabilized ZrO_2 containing different amounts of Nb_2O_5 after aging for 500 h at 220°C in air.

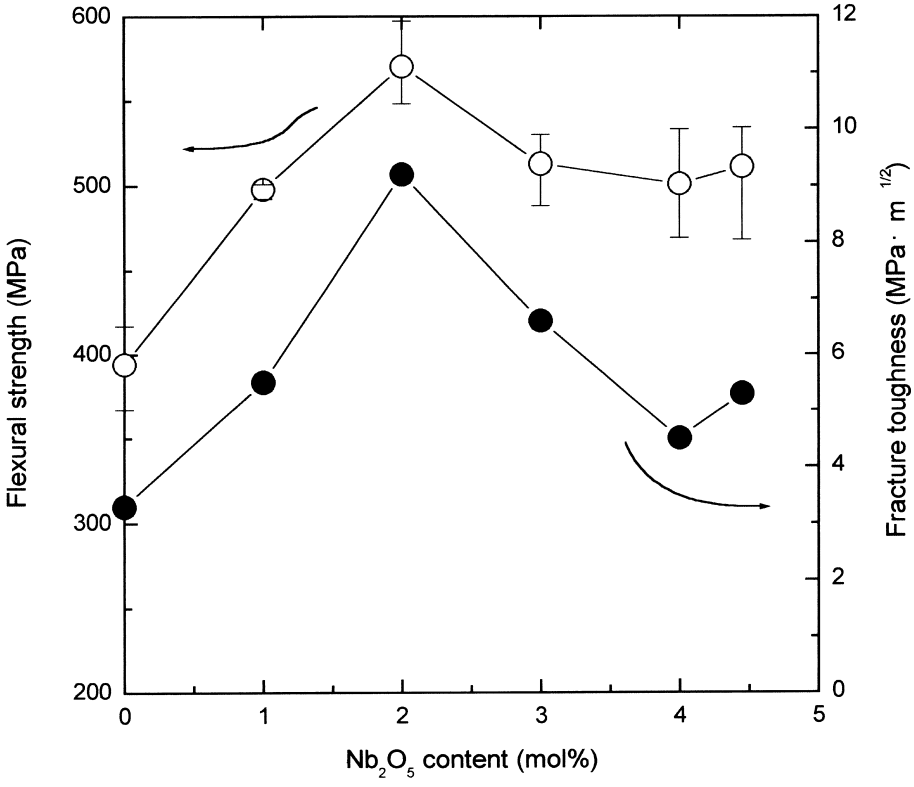

Fig. 4. Variation of biaxial strength and fracture toughness of 5.31 mol% Y_2O_3-stabilized ZrO_2 as a function of Nb_2O_5 content.

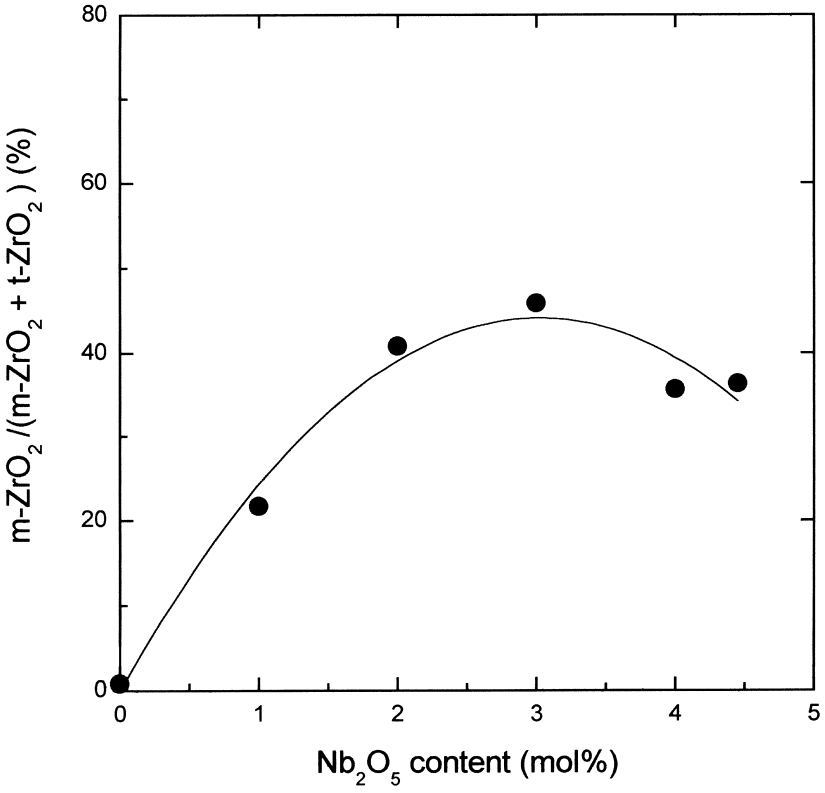

Fig. 5. m-ZrO_2 content on the fractured surfaces of 5.31 mol% Y_2O_3-stabilized ZrO_2 containing different amounts of Nb_2O_5.

Biaxial strength and fracture toughness were investigated and shown in Fig. 4. The initial increase of strength and fracture toughness probably stems from the fact that the stress-induced t→m phase transformation becomes significant due to the overwhelming contribution to mechanical properties by the degradable t-ZrO_2 compared to the stable t-phase. From 2 mol% Nb_2O_5, both strength and fracture toughness start to decrease, implying that the Nb_2O_5 content is just enough to form the tetrahedral bonds in the layer-like structure to relieve the internal strain, so that strength and toughness decrease as a result of lack of the stress-induced strengthening caused by the enhanced phase stability of the stable t-ZrO_2. The fraction of m-ZrO_2 on the fractured surfaces of 5.31Y–TZPs increases to 46% when the concentration increases to 3 mol% and then decreases slightly with increasing Nb_2O_5, as shown in Fig. 5. However, the fact that fracture toughness at 3 mol% Nb_2O_5 is lower than that at 2 mol% Nb_2O_5 implies the influence of increased phase stability on fracture toughness. The 46% m-ZrO_2 content that is related to the transformable t-phase does not increase with an increase in Nb_2O_5. Consequently, it is believed that most of t-ZrO_2 (4.45–4.6 mol% Nb_2O_5) may be present in the form of the stable t-ZrO_2 due to local Y–Nb odering, which is a prerequisite for TZP phase stability.

The effect of Nb^{5+} content on the Raman spectra of 5.31Y–TZP is shown in Fig. 6. The Nb doping shifts the Raman bands that are related with the stretching modes

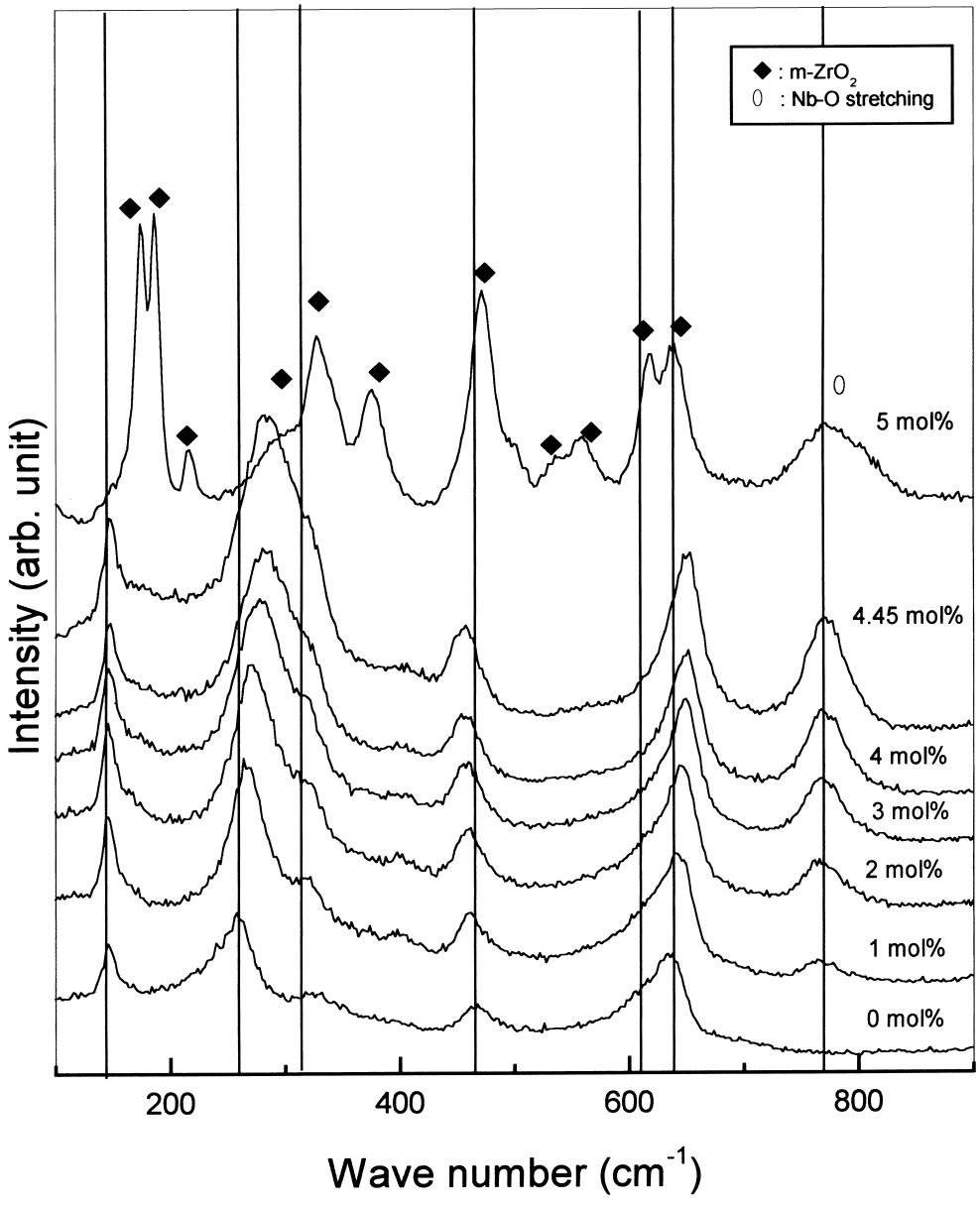

Fig. 6. Raman spectra of 5.31 mol% Y_2O_3-stabilized ZrO_2 containing different amounts of Nb_2O_5.

of Zr–O_{II} (260 cm^{-1}) and Zr–O_I (640 cm^{-1}) towards higher wavenumbers, which corresponds to the increase in zirconium–oxygen bond strength. The shift of Raman spectra indicates that a rather different local bonding environment with oxygens is formed due to the addition of Nb_2O_5. In addition to six Raman modes (147, 260, 321, 465, 609, 640 cm^{-1}) in t-ZrO_2, an extra peak near 770 cm^{-1} that is absent in 5.31Y–TZP appears and the peak height of 770 cm^{-1} increases linearly over the sum of peak height of 260 cm^{-1} and 640 cm^{-1} as the Nb_2O_5 content increases. However, the peak height of 770 cm^{-1} decreases as the Nb_2O_5 content is above 4.6 mol%. Hardcastle and Wachs [15] reported that the bond lengths and stretching frequencies for the perfect NbO_4 tetrahedron and the perfect NbO_6 octahedron are estimated to be 1.823±0.024 Å and 787±30 cm^{-1}, 1.977±0.024 Å and 586±30 cm^{-1}, respectively, under the assumption of the diatomic approximation and an anharmonic dependence between force constant and interatomic distance, and Raman band arising from symmetry related Nb–O modes always occur at low frequency below 300 cm^{-1}. A relatively large diffuse peak at around 780 cm^{-1}, characterized by Raman spectroscopy, was reported as the defect-fluorite phase in the Y_2O_3–Nb_2O_5 system [16]. It was argued that the diffuse Raman peaks were due to local ordering and a modulated structure through electron diffraction in the defect-fluorite solid solutions [16]. The Raman stretching frequency of the shortest Nb–O bond is observed only at 770 cm^{-1} that is 10 and 17 cm^{-1} lower than the value of 780 cm^{-1} for the defect-fluorite phase and 787 cm^{-1} for the ideal NbO_4 tetrahedron, respectively. As a result, it is in good agreement with the local Y–Nb ordered phase and the tetrahedral closest packing of O^{2-} ions around a Nb^{5+} ion. Several researchers [7,15] proposed that the coordination of Nb^{5+} should be changed from four to six during the t→m phase transformation, implying that the 770 cm^{-1} band should be shifted to 586 cm^{-1}. However, the 586 cm^{-1} Raman band is not observed in the present study. Failure to observe the 586 cm^{-1} band and the existence of the broad 770 cm^{-1} band at this composition suggests that although there occurs severe distortion of the NbO_4 tetrahedron because this phenomenon is commonly

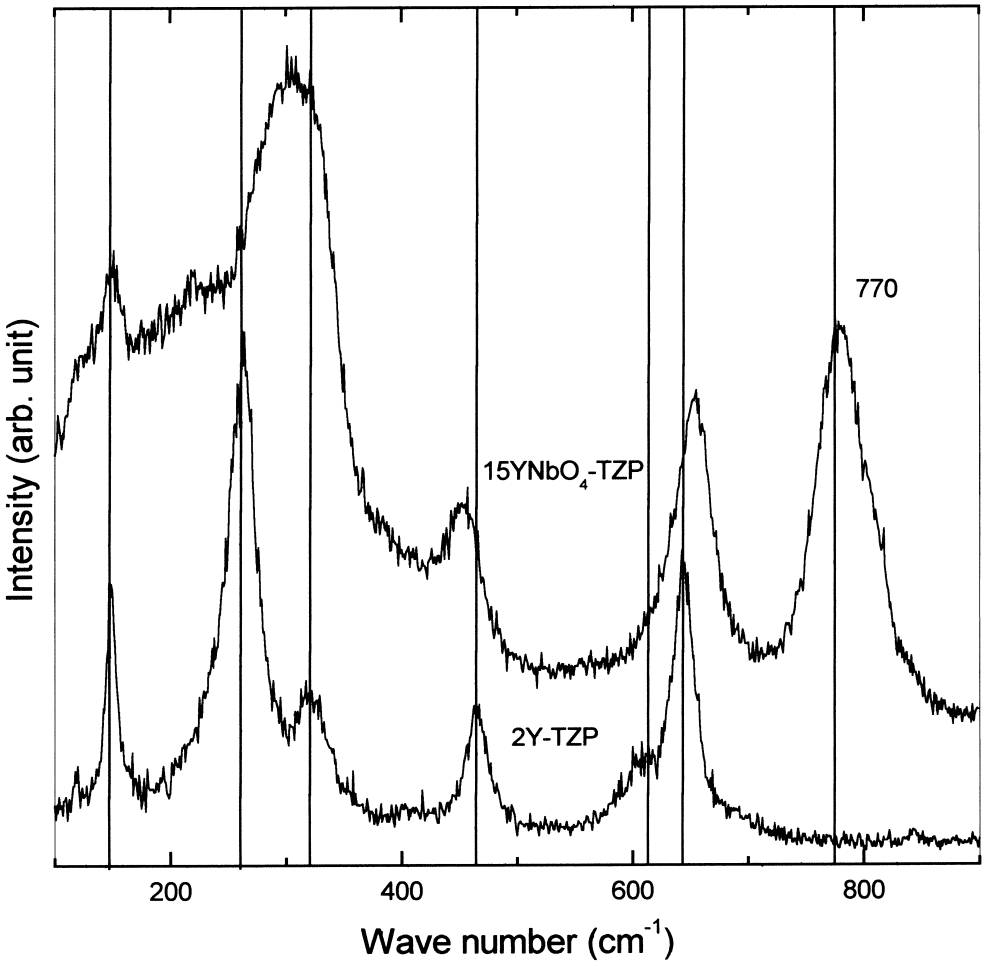

Fig. 7. Comparison of Raman spectra of 2 mol% Y_2O_3-stabilized ZrO_2 and 15 mol% $YNbO_4$-stabilized ZrO_2.

Table 1
Existing phases of (94.69−x) mol% ZrO_2; 5.31 mol% Y_2O_3; x mol% Nb_2O_5 samples sintered for 1 h at 1550°C in air. Resulting phases are characterized by Raman spectroscopy. C, T, Y, and M indicate cubic phase, tetragonal phase, defect-fluorite (Y–Nb ordered) phase, and monoclinic phase, respectively

Nb_2O_5 (mol%)	Resulting phases
0	C+T
1	C+T+Y
4.45	T+Y
4.6	T+Y
5	M+Y

observed when a disorder caused by the dopant addition is introduced into the crystal structure, the NbO_4 tetrahedron is sustained throughout the Nb_2O_5 concentration. Tyical Raman spectra of 2 mol% Y_2O_3-stabilized TZP (2Y–TZP) and 15 mol% $YNbO_4$-stabilized TZP (15 $YNbO_4$–TZP) are shown in Fig. 7. 2Y–TZP shows the typical six Raman modes which is unique for the fluorite structure, but the 770 cm^{-1} band, which is absent in the binary system Y_2O_3–ZrO_2, is observed in 15 $YNbO_4$–TZP as expected. The existing phases in 5.31Y–TZP doped with Nb_2O_5 characterized by Raman spectroscopy are summarized in Table 1. However, the fraction of the Y–Nb ordered phase could not be determined quantitatively in the present study.

4. Conclusions

Raman spectroscopy can identify the existing phases of cubic (c)-, tetragonal (t)-, monoclinic (m)-ZrO_2, and Y–Nb ordered phase in the ternary system (94.69−x) mol% ZrO_2; 5.31 mol% Y_2O_3; x mol% Nb_2O_5 ($x=0$–5 mol%). The phase stability of t-ZrO_2 may be governed by the competition between stable and transformable t-phase as a function of Nb_2O_5 content. Raman spectra of TZPs exhibit a broad and diffuse peak at around 770 cm^{-1} in contrast to the c-, t- and m-phase due to local ordering, which is likely to be related to the stable t-ZrO_2. Therefore, the phase stability of t-ZrO_2 in this system is attributed mainly to the Nb_2O_5 content.

References

[1] D.Y. Lee, D.-J. Kim, D.-H. Cho, Low-temperature phase stability and mechanical properties of Y_2O_3 and Nb_2O_5 co-doped tetragonal zirconia polycrystal ceramics, Journal of Materials Science Letters 17 (3) (1998) 185–187.
[2] D.Y. Lee, D.-J. Kim, J.-W. Jang, D.-W. Choi, S.-J. Lee, Phase stability of (Y,Nb)–TZP/Al_2O_3 composites under low temperature hydrothermal conditions, Materials Letters 39 (4) (1999) 221–226.
[3] C. Piconia, G. Maccauro, Zirconia as a ceramic biomaterial, Biomaterials 20 (1999) 1–25.
[4] D.-J. Kim, H.-J. Jung, D.-H. Cho, Phase transformation of Y_2O_3 and Nb_2O_5 doped tetragonal zirconia during low temperature ageing in air, Solid State Ionics 80 (1995) 67–73.
[5] D.-J. Kim, H.-J. Jung, J.-W. Jang, H.-L. Lee, Ionic conductivity, fracture toughness, and low temperature phase stability of tetragonal zirconia co-doped with Y_2O_3 and Nb_2O_5, Journal of American Ceramic Society 81 (9) (1998) 2309–2314.
[6] D.-J. Kim, Influence of aging environment on low-temperature degradation of tetragonal zirconia alloys, Journal of European Ceramic Society 17 (7) (1997) 897–903.
[7] P. Li, I. Chen, J.E. Penner-Hahn, Effect of dopants on zirconia stabilization — an X-ray absorption study: III. Charge–compensation dopants, Journal of American Ceramic Society 77 (5) (1994) 1289–1295.
[8] C. Quinn, R. Wusirika, Twinning in $YNbO_4$, Journal of American Ceramic Society 74 (2) (1991) 431–432.
[9] M.J. Mendelson, Average grain size in polycrystalline ceramics, Journal of American Ceramic Society 52 (8) (1969) 443–446.
[10] ASTM Standard F394-78, Biaxial flexure strength (modulus of rupture) of ceramic substrates, in: ASTM Annual Book of Standards, vol. 15.02, Section 15, American Society for Testing and Materials, Philadelphia, PA, 1996, pp. 446.
[11] P. Chantikul, G.R. Anstis, B.R. Lawn, D.B. Marshall, A critical evaluation of indentation techniques for measuring fracture toughness: II, strength method, Journal of American Ceramic Society 64 (9) (1981) 539–543.
[12] D.B. Marshall, T. Noma, A.G. Evans, A simple method for determining elastic-modulus-to-hardness ratios using Knoop indentation measurements, Communication of American Ceramic Society 65 (1982) C175–C176.
[13] R.C. Garvie, P.S. Nicholson, Phase analysis in zirconia systems, Journal of American Ceramic Society 55 (6) (1972) 303–305.
[14] D.-J. Kim, S.-H. Hyun, S.-G. Kim, M. Yashima, Effective ionic radius of Y^{3+} determined from lattice parameters of fluorite-type HfO_2 and ZrO_2 solid solutions, Journal of American Ceramic Society 77 (2) (1994) 597–599.
[15] F.D. Hardcastle, I.E. Wachs, Determination of niobium–oxygen bond distances and bond orders by Raman spectroscopy, Solid State Ionics 45 (1991) 201–213.
[16] M. Yashima, J.-H. Lee, M. Kakihana, M. Yoshimura, Raman spectral characterization of existing phases in the Y_2O_3–Nb_2O_5 system, Journal of Physics and Chemistry of Solids 58 (10) (1997) 1593–1597.